Thermal, Magnetic, and Optical Characteristics of ABS-Fe_2O_3 Nanocomposites

Gholamreza Nabiyouni,[1] Davood Ghanbari[2]

[1]*Department of Physics, Faculty of Science, Arak University, Arak 38156-88349, Iran*
[2]*Young researchers Club, Arak Branch, Islamic Azad University, Arak, Iran*

Received 19 June 2011; accepted 20 November 2011
DOI 10.1002/app.36514
Published online 1 February 2012 in Wiley Online Library (wileyonlinelibrary.com).

ABSTRACT: Uniform monodisperse FeOOH and hematite (Fe_2O_3) nanoparticles were synthesized at room temperature via a facile sonochemical reaction between $FeCl_3$ and NaOH. Fe_2O_3 nanoparticles were then added to acrylonitrile–butadiene-styrene (ABS) polymer. Nanoparticles and nanocomposites were characterized using X-ray diffraction, scanning electron microscopy, Fourier transform infrared, and photoluminescence (PL) spectroscopy techniques. The effect of the presence of FeOOH and Fe_2O_3 nanoparticles in the polymer matrix on the thermal properties was studied using thermogravimetric analysis and derivative thermogravimetric analysis, in both air and nitrogen atmospheres. The magnetic properties of the samples were also investigated using an alternating gradient force magnetometer. We found that the Fe_2O_3 nanoparticles exhibit a ferromagnetic behavior with a saturation magnetization of 0.869 emu/g and a coercivity of 191 Oe at room temperature. The coercivity of ABS/ Fe_2O_3 (5%) nanocomposites is found to be 252 Oe, higher than 226 Oe which is obtained for ABS/Fe_2O_3 (20%). © 2012 Wiley Periodicals, Inc. J Appl Polym Sci 125: 3268–3274, 2012

Key words: ABS; Fe_2O_3; FeOOH; sonochemical method; nanocomposite

INTRODUCTION

In the last two decades, nanostructure inorganic–polymer hybrids have been intensively studied due to the fact that they provide opportunities for preparation of novel composites that can be used in a wide range of applications such as: easy processability, low-cost manufacturing, and excellent thermal and mechanical properties. Polymer matrix nanocomposites have also been extensively investigated, since just a small amount of nanoparticles as an additive leads to production of novel high-performance materials with excellent physicochemical properties.[1–6] Hematite is an *n*-type semiconductor with a band gap of 2.1 eV and weak ferromagnetic properties in room temperature. It is extensively used as a catalyst, polishing agent, gas sensor, magnetic recording media, and color imaging. Iron oxides exhibit biocompatibility properties and have attracted attention in the field of biomedical applications such as clinical diagnosis, drug targeting, and enzyme immobilization.[7,8] The acrylonitrile–butadiene-styrene (ABS) is a thermoplastic polymer and is widely used because of its desirable properties and relatively low cost. ABS is composed of a styrene–acrylonitrile copolymer matrix and a grafted polybutadiene phase, which possesses easy processing (caused by polystyrene), good mechanical properties, thermal stability (caused by polyacrylonitrile), and improved impact strength (caused by polybutadiene).[9,10] The main disadvantage of ABS is flammability. Various methods for improving the fire retardancy of this copolymer have been developed.[11–19] Improvement in thermal stability is mainly achieved by adding halogen antimony synergism to the ABS polymer. Flame retardation is a process by which the normal degradation or combustion of polymers is changed. Application of the most current flame retardants is limited with respect to the environmental requirements, because of the toxic gases that are usually produced during the flaming reaction. Therefore, it is important to develop a new generation of flame retardants to substitute with the conventional flame retardants. The influence of ferric oxide nanoparticles on the thermal properties of several polymer matrixes such as polymethyl methacrylate, poly styrene and poly amide has been widely studied.[20–28] In this work, we report synthesis of FeOOH and hematite using sonochemical reaction. To study the influence of nanoparticles to the thermal properties of polymer matrix, the FeOOH and Fe_2O_3 nanoparticles were then incorporated in the ABS polymer. Magnetic properties of Fe_2O_3 nanoparticles and ABS/Fe_2O_3 nanocomposites were also compared.

Correspondence to: G. Nabiyouni (g-nabiyouni@araku.ac.ir).

Contract grant sponsor: Arak University Research Council; contract grant number: 89/5144

EXPERIMENTAL

Materials and methods

ABS polymer, $FeCl_3$ and dichloromethane were purchased from Aldrich Company. All the chemicals were used as received without further purifications. X-ray diffraction (XRD) patterns were recorded by a Rigaku D-max C III, X-ray diffractometer using Ni-filtered Cu Kα radiation. A multiwave ultrasonic generator (Bandeline MS 73), equipped with a converter/transducer and titanium oscillator, operating at 20 kHz with a maximum power output of 100 W was used for the ultrasonic irradiation. Scanning electron microscopy (SEM) images were obtained using a LEO instrument model 1455VP. Before taking images, the samples were coated by a very thin layer of Pt (using a BAL-TEC SCD 005 sputter coater) to make the sample surface conductor and proven charge accumulation, and obtaining a better contrast. Fourier transform infrared (FT-IR) spectra were recorded on Galaxy series FTIR5000 spectrophotometer. Thermogravimetric analysis (TGA) was carried out using an instrument (Shimadzu TGA 50H) with a heating rate of 10°C min^{-1} in both air and nitrogen atmospheres. The amount of sample used for TGA and derivative thermogravimetric analysis (DTG), under nitrogen atmosphere was about 1.9 mg, while about 1.35 mg of sample was used for similar experiment but performing under air atmosphere. Room temperature photoluminescence was studied by a Perkin Elmer fluorescence instrument. Room temperature magnetic properties were investigated using an alternating gradient force magnetometer (AGFM) device, made by Meghnatis Daghigh Kavir Company in an applied magnetic field sweeping between ±10,000 Oe.

Synthesis of Fe_2O_3 nanoparticles

First 1 g of $FeCl_3$ is dissolved in 100 mL of distilled water. Then 50 mL of NaOH solution 0.2*M* is slowly added to the solution, under ultrasonic waves (75 W) for 30 min. A brown precipitate is obtained confirming the synthesis of FeOOH. The precipitate of FeOOH is then centrifuged and rinsed with distilled water, followed by being left in an atmosphere environment to dry. The brown powder (obtained in this stage) is then calcinated at 400°C in an oven for 4 h. Thereupon, the precipitate colour goes from brown to red, confirming production of ferric oxide. Figure 1 shows the schematic diagram for experimental setup used for this sonochemical reaction.

Preparation of ABS nanocomposites

First 1 g of ABS is dissolved in 10 mL dichloromethane solution. Then 0.2 g of nanoparticles (either Fe_2O_3 or FeOOH) is separately dispersed in 10 mL dichloromethane solution with ultrasonic waves. The nanoparticles dispersion is then slowly added to the polymer solution. The new solution is then mixed and stirred for 6 h. The product is casted on a glass plate and is left for 2 h in order for the solvent to evaporate.

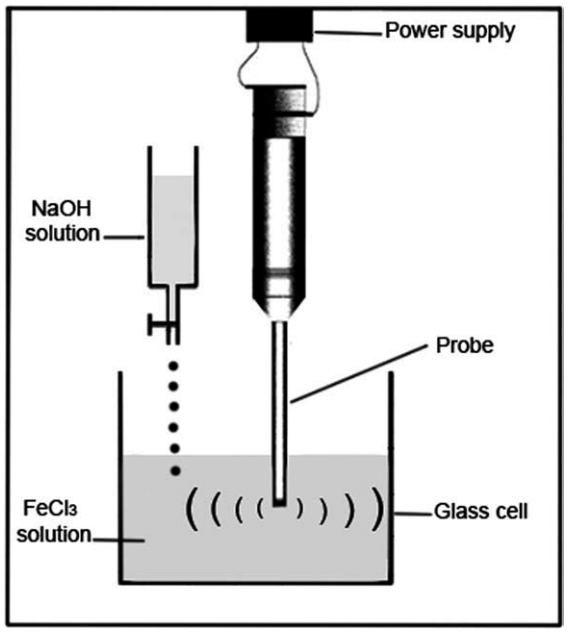

Figure 1 Schematic diagram for the experimental setup used for the sonochemical reactions.

RESULTS AND DISCUSSION

The XRD pattern of FeOOH and Fe_2O_3 nanoparticles are shown in Figure 2(a,b), respectively. The XRD pattern of as-prepared FeOOH nanoparticles is indexed as a pure orthorhombic phase (space group: Pbnm) which is very close to the literature values (JCPDS No. 81-0464), the narrow sharp peaks indicate that the Fe_2O_3 nanoparticles are well crystallized. The XRD pattern of Fe_2O_3 nanoparticles is indexed as a rhombohedral phase (space group: R-3c) and it is close to the literature values (JCPDS No. 79-1741). The excitation and emission photoluminescence spectra of the samples are shown in Figure 3(a,b), respectively. PL spectrum of Fe_2O_3 is recorded at the excitation wavelength of 293.29 nm, and its PL spectrum consists of a strong peak at 398 nm which can be ascribed as a high level transition in Fe_2O_3 nanoparticles, while the PL spectrum of ABS/Fe_2O_3 with excitation wavelength of 333.59 nm, consists of a strong peak at 390 nm. It has been reported that this kind of band edge luminescence arises from the recombination of exactions and/or shallowly trapped electron–hole pairs.[29]

The SEM image of FeOOH nanoparticles is shown in Figure 4(a). Figure 4(b) gives the SEM image of

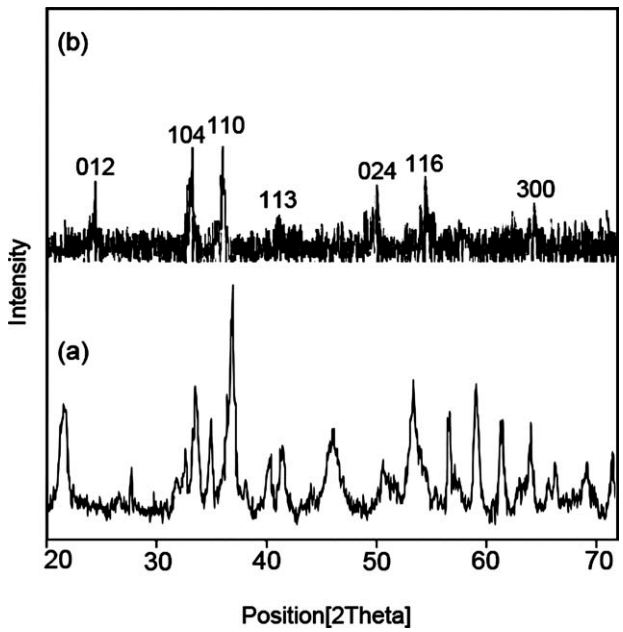

Figure 2 XRD patterns of (a) FeOOH and (b) Fe_2O_3 nanoparticles.

Fe_2O_3 nanoparticles. Figure 4(c) shows the SEM image of the pure ABS surface. Figure 4(d) shows the SEM image of ABS/FeOOH nanocomposite, indicating that the FeOOH nanoparticles are well dispersed in the ABS matrix. Figure 4(e,f) show SEM images of ABS/Fe_2O_3 (5% and 20%, respectively) and confirm the existence of Fe_2O_3 nanoparticles in the polymeric matrix. Figure 5(a) shows the FTIR spectrum of as-prepared FeOOH nanoparticles and exhibits two absorption peaks around 3237 cm^{-1} and 1453 cm^{-1}, corresponding to the stretching and bending modes of OH, respectively. The peak at 626 cm^{-1} corresponds to the Fe—O bond in FeOOH.[30] FTIR spectrum of ABS/FeOOH nanocomposite is shown in Figure 5(b). In the ABS matrix, the absorption which takes place at the wave number of 2238 cm^{-1}, is related to the nitrile groups in the polymer. Two absorption peaks in the wave numbers 1448 and 1600 cm^{-1} are referred to the aromatic ring stretching in the ABS, while the absorption peaks at 2928 cm^{-1} and 3027 cm^{-1} are attributed to the vibrations of aliphatic and aromatic C—H bonds, respectively.[31] The bands at 557 cm^{-1} and 621 cm^{-1} have been attributed to the presence of FeOOH in the nanocomposite. Figure 5(c) shows FTIR spectrum of Fe_2O_3 nanoparticles and exhibits two strong bands at 531 and 450 cm^{-1} attributing to the Fe—O bond in Fe_2O_3.[32] The 3430 cm^{-1} absorption peak could be due to the water molecules adsorbed on the Fe_2O_3 nanoparticles. FTIR spectrum of ABS/Fe_2O_3 nanocomposite is shown in Figure 5(d). Except for which exists in the ABS or Fe_2O_3, no additional absorption peak is observed in this spectrum. Characteristic absorption peaks for the ABS/FeOOH and ABS/Fe_2O_3 nanocomposites are shown in Table I.

TGA with the heating rate of 10°C/min under nitrogen atmosphere have been performed on the samples. TGA curves of pure polymer, ABS/FeOOH and ABS/Fe_2O_3 (with weight percent of 5 and 20)

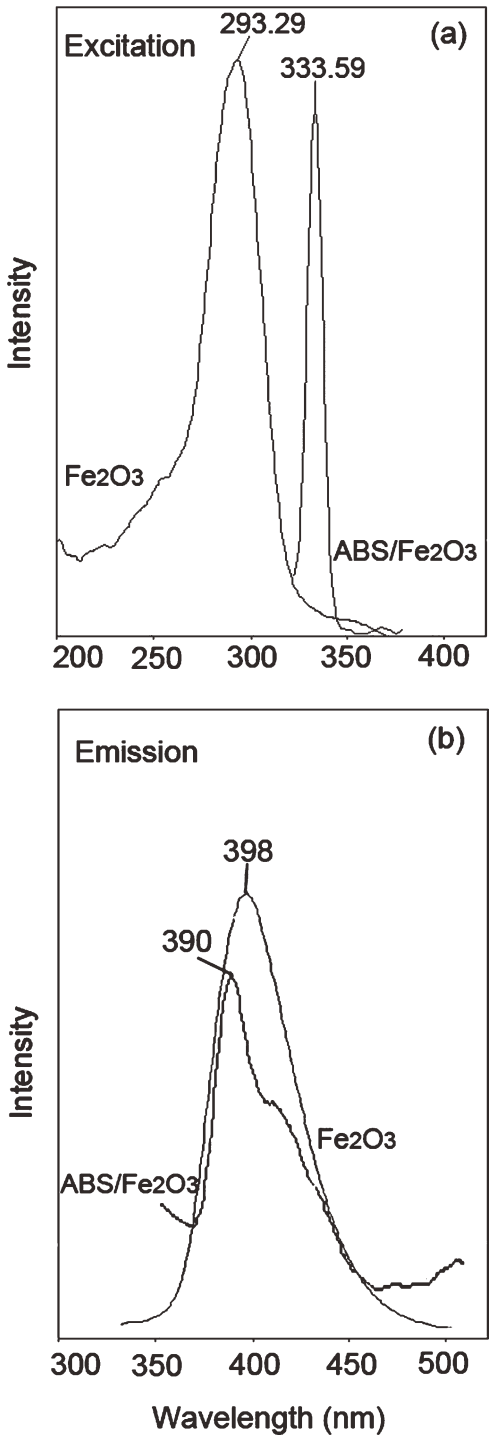

Figure 3 (a) Excitation spectra of Fe_2O_3 nanoparticles and ABS/Fe_2O_3 nanocomposite, (b) room temperature photoluminescence spectra of Fe_2O_3 nanoparticles and ABS/Fe_2O_3 nanocomposite.

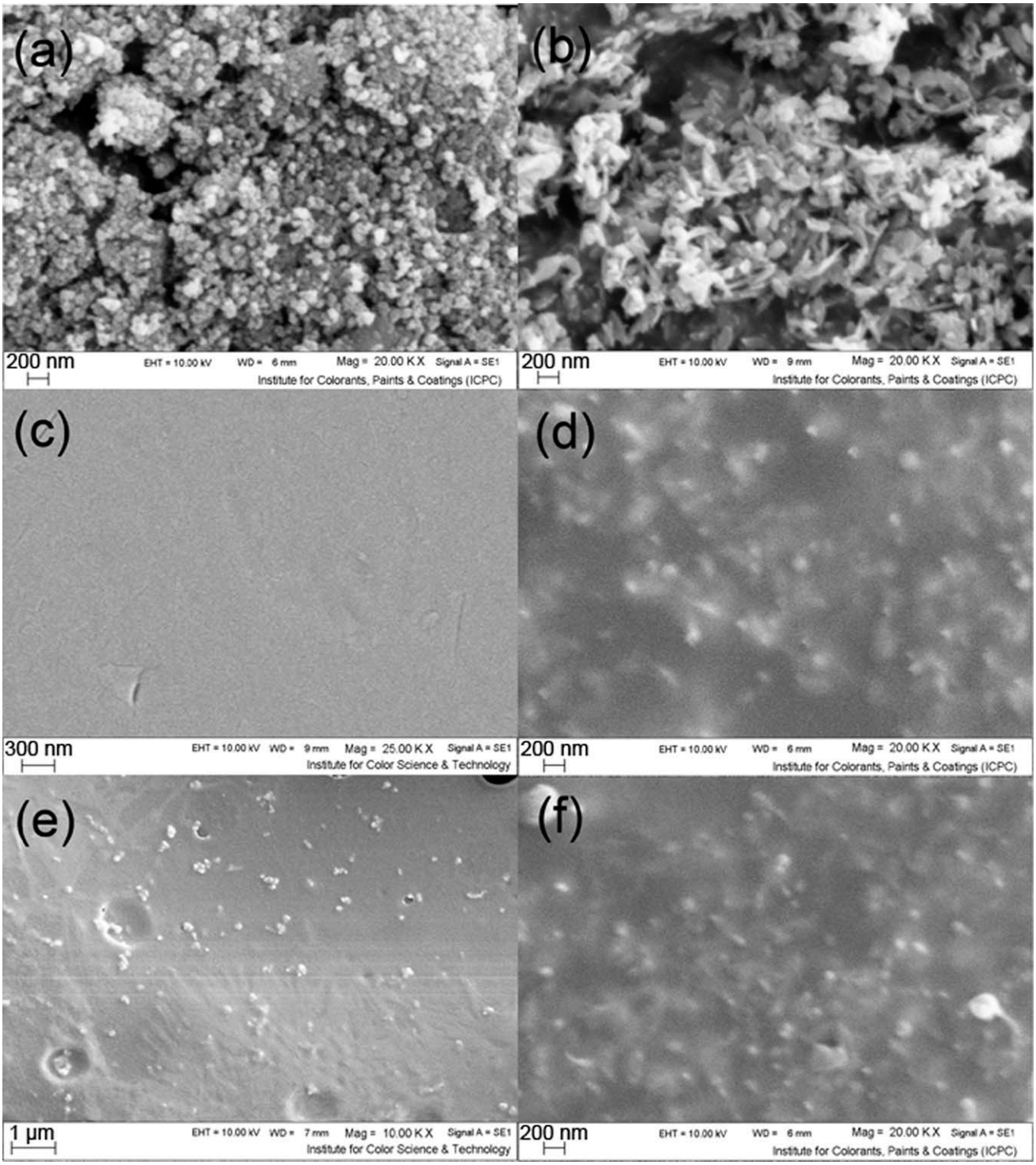

Figure 4 SEM images of (a) FeOOH nanoparticles, (b) Fe_2O_3 nanoparticles, (c) pure ABS, (d) ABS/FeOOH(20%), (e) ABS/Fe_2O_3 (5%), and (f) ABS/Fe_2O_3 (20%).

are shown in Figure 6(a–d). DTG graphs, presenting the temperature of maximum weight-loss rate (T_{max}) for pure ABS and ABS/Fe_2O_3 (5% and 20%) are shown in Figure 7.

Results from TGA and DTG data indicate that adding of Fe_2O_3 to the polymeric matrix leads to a reduction of the initial degradation temperature (T_{onset}) but enhances the residue at the temperatures above 550°C. T_{onset} and T_{max} for pure ABS and its composites, as well as the percentage of residue material and the real proportion of nanoparticles added to the pure polymer matrix, are summarized in Table II. As the Figures 6 and 7 indicate, just one step decomposition around 385–475°C is found for pure

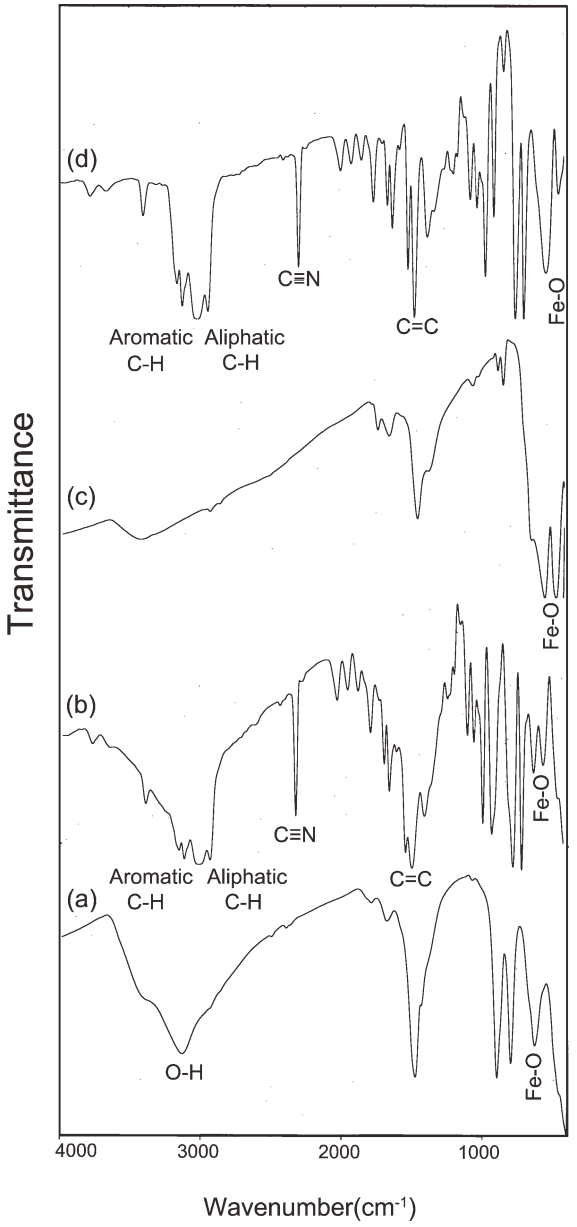

Figure 5 FT-IR spectrum of (a) FeOOH nanoparticles, (b) ABS/FeOOH nanocomposite, (c) Fe_2O_3 nanoparticles, and (d) ABS/Fe_2O_3 nanocomposite.

TABLE I
Characteristic Absorbance Bands for ABS/FeOOH Nanocomposite and ABS/Fe_2O_3 Nanocomposite in the Range of 400–4000 cm^{-1}

Band assignment	ABS/FeOOH	ABS/Fe_2O_3
Aromatic C—H stretching	3027	3027
Aliphatic C—H stretching	2928	2925
C≡N stretching	2238	2238
Aromatic ring stretching	1600	1601
Aromatic ring stretching	1448	1448
Aromatic C—H in plane bending	1026	1027
Aromatic C—H out of plane bending	762	761
Aromatic C—H out of plane bending	702	702
Fe—O	621	552
Fe—O	557	471

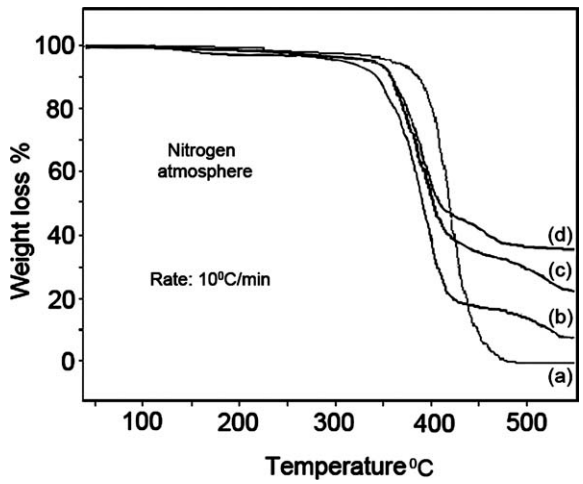

Figure 6 TGA curves of (a) pure ABS, (b) ABS/Fe_2O_3 (5%), (c) ABS/Fe_2O_3 (20%), and (d) ABS/FeOOH (20%) under nitrogen atmosphere.

ABS under nitrogen atmosphere, while the DTG results of polymer nanocomposites exhibit two steps degradation.

Enhancement on residue material of composites can be assigned to the adsorption of polymer chains onto the Fe_2O_3 and FeOOH surfaces leading to decrease the segmental mobility. Exfoliated nanoparticles act as barriers which slow down product volatilization and thermal transport during decomposition of the polymer.[9,10,33]

TGA and DTG graphs of pure ABS, ABS/Fe_2O_3 (20%) with the heating rate of 10°C/min under the air atmosphere are given in Figures 8 and 9, respectively. Adding Fe_2O_3 to the ABS also leads to a small reduction of the T_{onset} but enhances the residue at the temperatures above 600°C. The results are summarized in Table III.

Room temperature magnetic properties of our samples are studied using an AGFM device. Hysteresis loops for Fe_2O_3 nanoparticles and ABS/Fe_2O_3

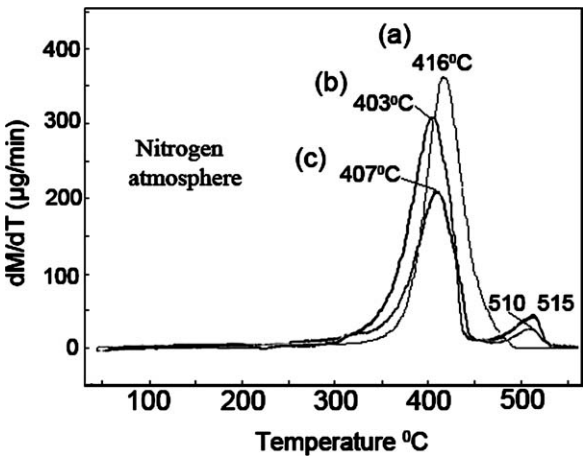

Figure 7 DTG curves of (a) pure ABS, (b) ABS/Fe_2O_3 (5%), and (c) ABS/Fe_2O_3 (20%) under nitrogen atmosphere.

TABLE II
The Summarized TGA and DTG Results Taken from Figures 6 and 7

Sample	T_{onset}[a]	T_{max}[b] Step 1	T_{max} Step 2	Real proportion[c]	Residue at 550°C (%)[d]
ABS	385	416	–	–	0.2
ABS/Fe_2O_3 5%	340	403	510	4.7	8
ABS/Fe_2O_3 20%	355	407	515	16.6	23
ABS/FeOOH 20%	355	408	460	16.6	35

[a] Initial decomposition temperature.
[b] Maximum weight-loss temperature.
[c] Real proportion of nanoparticles added to the pure polymer matrix. For example for ABS/Fe_2O_3, 0.2 g Fe_2O_3 was added to 1 g ABS. Thus the total sample weight is 1.2 g, and real proportion is (0.2/1.2) or 16.6%.
[d] Weight percentage of material left after TGA analysis at maximum temperature of 550°C in N_2 atmosphere.

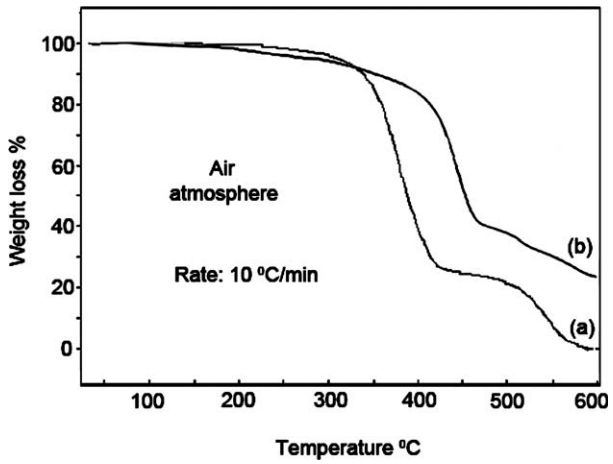

Figure 8 TGA curves of (a) pure ABS and (b) ABS/Fe_2O_3 nanocomposite, under air atmosphere.

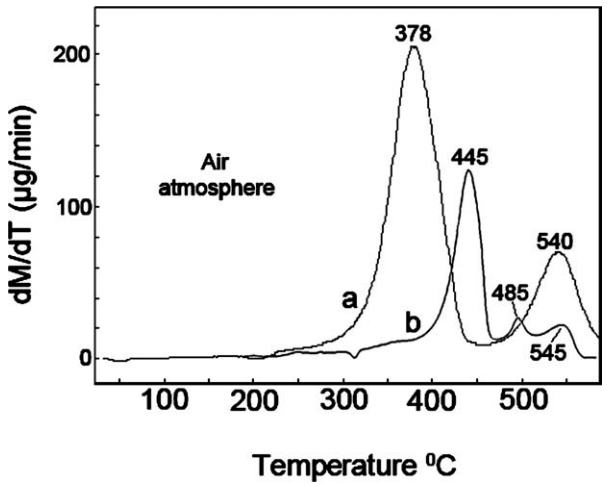

Figure 9 DTG curves of (a) pure ABS and (b) ABS/Fe_2O_3 (20%) under air atmosphere.

(5 and 20%) nanocomposite are depicted in Figure 10(a–c), respectively. The hysteresis loops of the hematite nanoparticles and nanocomposites show a weak ferromagnetic behavior. Coercivity, remanence, and saturation magnetization of the synthesized samples are listed in Table IV. The saturation magnetization of Fe_2O_3 nanoparticles is much higher than those are obtained for ABS/Fe_2O_3 (5 and 20%) nanocomposites. The results also indicate that forming the nanocomposite and distribution of the magnetic nanoparticles into the polymer matrix leads to increase the coercivity. The coercivity of ABS/Fe_2O_3 (5%) nanocomposites is also higher than which is obtained for ABS/Fe_2O_3 (20%). This result can be attributed to the interactions between polymer chains of ABS and Fe_2O_3 nanoparticles.

CONCLUSIONS

To enhance the thermal properties, many nanocomposites based on ABS polymers have been synthesized by adding different additives such as PbS, SnS, and halogenated compounds.[9,10,13] However, most of these additives are toxic and environmentally non-friendly. In this work, we introduce synthesis of new non-toxic magnetic nanoparticles for producing of a new ABS polymeric nanocomposite. FeOOH nanoparticles are synthesized via a simple sonochemical reaction. The

TABLE III
The Summarized TGA and DTG Results Taken from Figures 8 and 9

Sample	T_{onset}	T_{max} Step 1	T_{max} Step 2	T_{max} Step 3	Real proportion	Residue at 600°C (%)
ABS	350	378	540	-	0	0.2
ABS/Fe_2O_3 20%	250	445	485	545	16.6	23

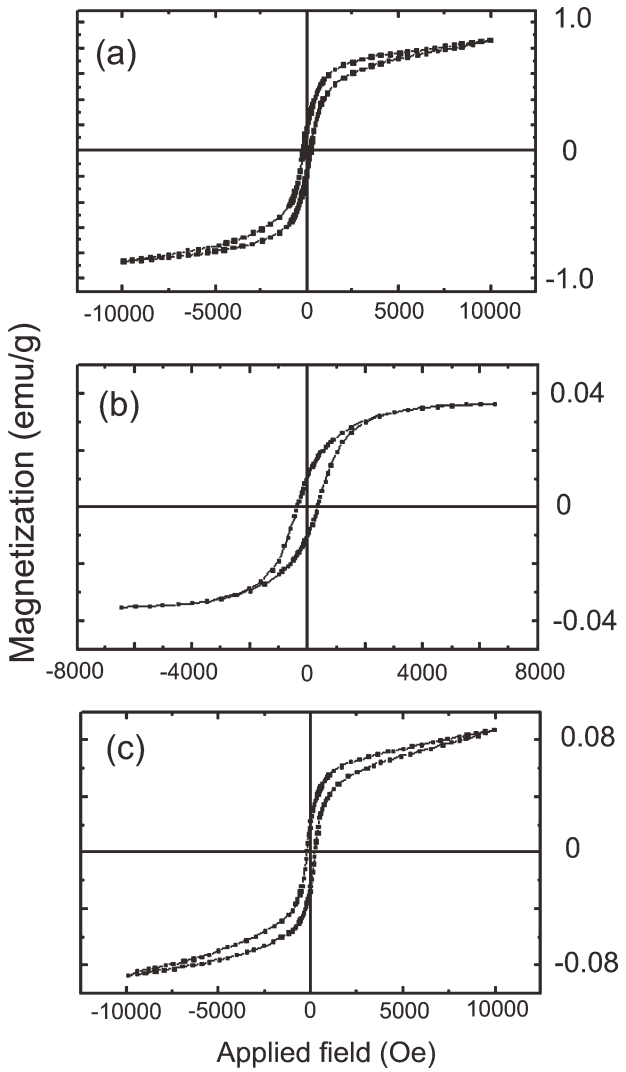

Figure 10 Room temperature magnetization curves of (a) Fe_2O_3 nanoparticles, (b) ABS/Fe_2O_3 (5%), and (c) ABS/Fe_2O_3 (20%) nanocomposite.

synthesized FeOOH nanomaterials are then converted into hematite (Fe_2O_3) by the calcination method. It was found that the as-obtained Fe_2O_3 nanoparticles exhibit a ferromagnetic behavior with a saturation magnetization of 0.869 emu/g and a coercivity of 191 Oe at room temperature. The influence of presence of nanoparticles on the thermal properties of ABS matrix was also studied. The thermal stability of the nanocomposites changes in the presence of the nanoparticles.

TABLE IV
Coercivity, Remanence, and Saturation Magnetization of the Fe_2O_3 Nanoparticles and ABS/Fe_2O_3 (5 and 20%) Nanocomposites

Sample	Saturation magnetization (emu/g)	Coercivity (Oe)	Remanence (emu/g)
Fe_2O_3	0.869	191	0.178
ABS/Fe_2O_3 5%	0.036	252	0.010
ABS/Fe_2O_3 20%	0.087	226	0.024

The authors appreciate Ms Niloufar Nabiyouni for English assistance.

References

1. Dudic, D.; Marinovic-Cincovic, M.; Nedeljkovic, J. M.; Djokovic, V. Polymer 2008, 49, 4000.
2. Mouritz, A. P.; Gibson, A. G. Fire Properties of Polymer Composite Materials; Springer: Dordrecht, 2006.
3. Laoutid, F.; Bonnaud, L.; Alexandre, M.; Lopez-Cuesta, J.; Dubois, Ph. Mater Sci Eng R 2009, 63, 100.
4. Morgan, A. B.; Wilkie, C. A. Flame Retardant Polymer Nanocomposite; Wiley: New Jersey, 2007.
5. Hull, T. R.; Kandola, B. K. Fire Retardancy of Polymers New Strategies and Mechanisms; RSC: Cambridge, 2009.
6. Horrocks, A. R.; Price, D. Fire Retardant Materials; Woodhead: Cambridge, 2001.
7. Hassanjani-Roshan, A.; Vaezi, M. R.; Shokuhfar, A.; Rajabali, Z. Particuology 2011, 9, 95.
8. Gupta, R. K.; Ghosh, K.; Dong, L.; Kahol, P. K. Mater Lett 2010, 64, 2132.
9. Yousefi, M.; Gholamian, F.; Ghanbari, D.; Salavati-Niasari, M. Polyhedron 2011, 30, 1055.
10. Yousefi, M.; Salavati-Niasari, M.; Gholamian, F.; Ghanbari, D.; Aminifazl, A. Inorg Chim Acta 2011, 371, 1.
11. Owen, S. R.; Harper, J. F. Polym Degrad Stab 1999, 64, 449.
12. Choi, Y. S.; Xu, M.; Chung, I. J. Polymer 2005, 46, 531.
13. Bhaskar, T.; Murai, K.; Matsui, T.; Brebu, M. A.; Uddin, M. A.; Muto, A.; Sakata, Y.; Murata, K. J. Anal Appl Pyrolysis 2003, 70, 369.
14. Czegeny, Z.; Blazso, M. J. Anal Appl Pyrolysis 2008, 81, 218.
15. Hoang, D.; Kim, J. Polym Degrad Stab 2008, 93, 36.
16. Ma, H.; Tong, L.; Xu, Z.; Fang, Z.; Jin, Y.; Lu, F. Polym Degrad Stab 2007, 92, 720.
17. Nguyen, C.; Kim, J. Polym Degrad Stab 2008, 93, 1037.
18. Cai, Y.; Hu, Y.; Song, L.; Xuan, S.; Zhang, Y.; Chen, Z.; Fan, W. Polym Degrad stab 2007, 92, 490.
19. Lee, K.; Kim, J.; Bae, J.; Yang, J.; Hong, S.; Kim, H. K. Polymer 2002, 43, 2249.
20. Dzunuzovic, E.; Marinovic-Cincovic, M.; Jeremic, K.; Vukovic, J.; Nedeljkovic, J. Polym Degrad Stab 2008, 93, 77.
21. Ninjbadgar, T.; Yamamoto, S.; Takano, M. Solid State Sci 2005, 7, 33.
22. Marinovic-Cincovic, M.; Popovic, M. C.; Novakovic, M. M.; Nedeljkovic, J. M. Polym Degrad Stab 2007, 92, 70.
23. Marinovic-Cincovic, M.; Saponjic, Z.; Djokovic, V.; Milonjic, S.; Nedeljkovic, J. M. Polym Degrad Stab 2006, 91, 313.
24. Kuljanin, J.; Marinovic-Cincovic, M.; Zec, S.; Comor, M.; Nedeljkovic, J. M. J Mater Sci Lett 2003, 22, 235.
25. Laachachi, A.; Cochez, M.; Ferriol, M.; Lopez-Cuesta, J. M.; Leroy, E. Mater Lett 2005, 59, 36.
26. Laachachi, A.; Leroy, E.; Cochez, M.; Ferriol, M.; Lopez-Cuesta, J. M. Polym Degrad Stab 2005, 89, 344.
27. Liang, Y.; Xia, X.; Luo, Y.; Jia, Z. Mater Lett 2007, 61, 3269.
28. Yang, S.; Castilleja, J. R.; Barrera, E. V.; Lozano, K. Polym Degrad Stab 2004, 83, 383.
29. Salavati-Niasari, M.; Ghanbari, D.; Davar, F. J. Alloys Compd 2009, 488, 442.
30. Yan, H.; Zhang, B. Mater Lett 2011, 65, 815.
31. Ebadi Amooghin, A.; Sanaeepur, H.; Moghadassi, A.; Kargari, A.; Ghanbari, D.; Sheikhi Mehrabadi, Z. Sep Sci Technol 2010, 45, 1385.
32. Janardhanan, S. K.; Ramasamy, I.; Nair, B. U. Trans Met Chem 2008, 33, 127.
33. Kuljanin, J.; Marinovic-Cincovic, M.; Stojanovic, Z.; Krkljes, A.; Abazovic, N. D.; Comor, M. I. Polym Degrad Stab 2009, 94, 891.